EFFECTS OF UV EXPOSURE ON STRUCTURAL HEALTH MONITORING CAPABILITIES OF EPOXY/CNT COMPOSITE BINDERS

Joseph Cunningham
Advisor: Dr. Gary D. Seidel
Virginia Polytechnic Institute and State University, Blacksburg, VA 24060

Abstract

Upcoming NASA missions have increased the drive for development of multi-functional materials for Lunar surface deployment. Structural health monitoring (SHM) functionality may be achieved through the incorporation of carbon nanotubes (CNTs) into polymer matrices, which may be used as binders in structural composites. Polymeric materials may experience significant degradation when exposed to high dosages of ultraviolet (UV) radiation, an issue exacerbated by long exposure periods and the extremely thin Lunar atmosphere. CNT inclusions tend to retard damaging UV effects in polymer composites, but the influence of this exposure on SHM capabilities has not yet been documented. In this research, epoxy/1% MWCNT ASTM D695 composite compression samples were subjected to quasi-static mechanical testing and electrical monitoring both with and without UV exposure. Compression occurred at 1.3 mm/min while 10kHz, 2V AC was passed through attached electrodes. Resistance and reactance were recorded via a custom LabView program, and MATLAB was used to identify relationships between stress/strain and normalized electrical behavior. Strain, microdamage, and macrodamage sensing were noted in both sample categories, though UV exposed samples showed distinct differences when compared with unexposed samples.

Introduction

The advent of the Artemis Program has led to increased emphasis on materials, technologies and processes necessary to make a human presence on the Moon both safe and sustainable[1]. Nanomaterials have been specifically recommended as a way in which structural stability and safety may be increased, in part through the design of self-sensing and structural health monitoring (SHM) properties into novel material concepts[2].

In SHM, structural members are monitored either periodically or continuously for evidence of damage which may lead to overall structural failure[3]. Various methods may be used to carry out this task, including visual inspection[3,4], vibration analysis[3], application of discrete sensors[4], or in-situ material self-sensing[5–8]. In-situ sensing eliminates both the need for direct inspection and simplifies sensing requirements, as internal material states may be identified directly electrical response[5–8]. This type of sensing may be achieved through incorporation of carbon nanomaterials, such as nanotubes (CNTs) or graphene nanoplatelets (GNPs), into polymer matrices[9,10]. Specifically, low CNT mass fraction polymer binders have been used to detect both strain and damage in this manner[6,8,11,12].

If self-sensing CNT/polymer composites are to be applied to Lunar projects, an understanding of their behavior under intense UV exposure is necessary. Polymeric materials experience changes in mechanical and solubility properties[13,14], changes in thermal properties[15] and mass loss[15,16] when exposed to significant dosages of UV radiation, which can be detrimental to their functionality. However, when small proportions of CNTs are dispersed within a polymer matrix, degradation effects decrease, in part due to the for-

mation of an entangled CNT network on exposed surfaces[17,18]. These effects might serve to lessen the severity of UV degradation effects on the Lunar surface, where exposure can be as high as 107 W/m^2 (when reflective and thermal conditions are not accounted for)[19] for ~93% of the time in South Polar areas[20] such as those targeted by Artemis. For comparison, at Earth's surface this exposure drops to around 35 W/m^2 with much shorter durations[21].

The effect of UV induced surface CNT networks and other UV effects on SHM properties of self-sensing CNT/polymer composites has not previously been investigated, and it is this gap which this research seeks to fill.

Methodology

MWCNT Composite Fabrication

The binder selected for this study is a 79.1% Epon-862/20.9% Curing agent W system[22] with compositional similarities to low-temperature epoxies[23,24]. MWCNTs were obtained from Cheaptubes.com and have an outer diameter of 20-30 nm, inner diameter of 5-10 nm, length of 10-30 μm, and electrical conductivity of >100 S/cm, with >95% purity and <1.5% ash content by weight.

The predetermined amount of CNTs was first dispersed in 100 mL of acetone by hand mixing, after which this slurry was subjected to bath sonication for two cycles of 30-min each at 20-sec pulse, 5-sec delay, and 25% amplitude. The Epon-862 was then hand mixed into this slurry, after which another two cycles of sonication were carried out to ensure dispersion of CNTs. After sonication, the acetone was stripped from the mixture using a rotary evaporator on a 60 minute cycle in an 80 °C water bath at a vacuum pressure of 250 mb. Curing Agent W was then added and hand mixed after which the composite was degassed for 30 minutes at ~90 kPa vacuum pressure before being poured into preheated, degassed silicone molds (pre-sprayed

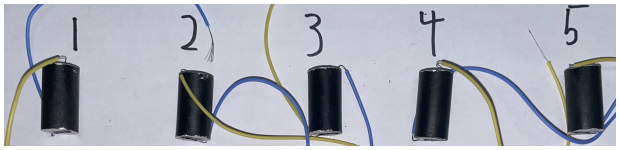

Figure 1: Epoxy/CNT samples with electrodes.

with mold release agent) and degassed for another cycle. A two-part curing process was then carried out in a vacuum oven, with two hours at 121 °C followed by two hours at 176 °C. Completed samples (including electrodes, discussed below) can be seen in Fig. 1.

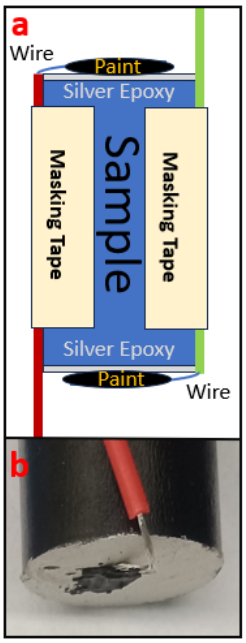

Figure 2: a) Construction diagram and b) finished electrode.

After removal from molds, samples were sanded to assure perpendicularity of circular faces. Sample masses were recorded, and void estimates were made based on expected mass of composite filling sample volume. Specimens to be exposed to UV were subjected to 288 or 576 hour exposure times within the custom UV chamber (see UV Exposure, below).

Electrodes were then created on both faces of each specimen using a thin layer of silver conductive epoxy[25]. Two silicone-insulated, stranded tinned copper wires were stabilized on the sides of each specimen using masking tape, after which they were bend down to the conductive epoxy surface and attached with conductive paint (see Fig. 2). The tape was then removed and sample dimensions taken in preparation for testing.

UV Exposure

For a standing Lunar structure, UV exposure (100-400 nm wavelength range)[26] is es-

timated at 113 (W/m^2)[19,27–29]. The custom UV chamber detailed in previous work[30] provides an exposure spectrum >290 nm similar to those which have been proven to generate entangled surface CNT networks (295-400 nm wavelengths)[18]. Chamber photons carry sufficient energies to break covalent bonds found in the Epon-862 system[31–34], making degradation and surface network growth likely. C-C backbone bonds are especially susceptible, as all wavelengths below 346 nm have the potential to cause chain scission.

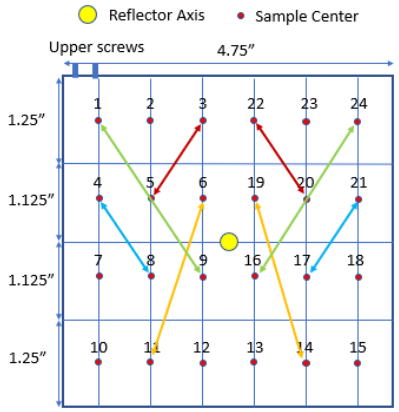

Figure 3: Sample rotation scheme to allow even exposures.

To enable exposures to be consistent (within ±5% relative to other samples in the exposure cycle), a rotation scheme was developed based on areas of higher or lower irradiance within the chamber (positions near the center had higher irradiance values than those near the edges. See Fig. 3). For the 576 hr (∼500MJ/m^2) exposures noted here, samples were rotated 1/4 rotation after 144 hours, positions were switch at 288 hours, another 1/4 rotation was executed at the new positions at 432 hours, and samples were removed from the enclosure at 576 hours.

Mechanical and Electrical Testing

In preparation for testing, non-conductive paper layers were taped to each platform on an Instron uniaxial testing rig. Thin pieces of aluminum plate were placed on these sheets to keep them from being punctured by epoxy samples (see Fig. 4). Samples were placed on this insulation, and after preloading to 1-2 N, baseline resistance and reactance measurements were taken using an LCR meter set to a frequency of 10 kHz and voltage of 2 V. Samples were then further preloaded to between 4 and 6 N, and mechanical compressive testing and electrical data captured was instigated simultaneously. A crosshead displacement rate of 1.3 mm/min was utilized to keep testing within the quasistatic regime. At test conclusion, electrical data capture was stopped and recorded.

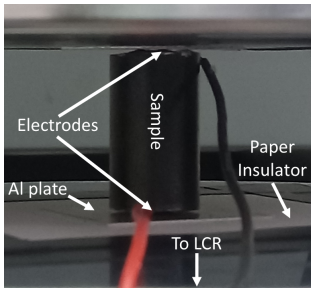

Figure 4: PBRC sample in Instron uniaxial testing rig. Note electrodes attached to sample top and bottom.

Data Analysis

Mechanical and electrical data was tabulated, correlated relative to elapsed test time, and interpolated to allow single values resistance, reactance and stress to be associated with specific strain values and enable comparison and plotting of these metrics with strain progression. Methods were devised for identifying various regions of interest (linear, damage onset, microdamage dominated, and macrodamage dominated) using standard MATLAB functions and fitting tools.

Normalized change in resistance (NCR) and normalized change in reactance (NCX), important metrics of interest for in-situ SHM, are calculated as in Eqs. 1-2 below, where R is resistance and X is reactance, while values with a 0 subscript represent unstrained, reference values of resistance and reactance, respectively:

$$NCR = \frac{R - R_0}{R_0} \tag{1}$$

$$NCX = \frac{X - X_0}{X_0} \quad (2)$$

Previous research has shown that these general metrics allow correlation between instantaneous material responses and concurrent electrical data[5,7,8], so they will be the primary indicators in this paper.

Results

Two sample fabrications were undertaken, yielding 18-20 samples each. Half of these samples were exposed to ~500 MJ/m^2 of UV radiation, while the control groups were not. Example mechanical and associated electrical results gleaned from one such set of exposed and unexposed samples is shown in Fig. 5. Results from two unexposed samples are shown in a-b, while those from two ~500MJ/m^2 samples are shown in c-d. NCR response can be seen in subfigures a) and c) while NCX response is noted in b) and d). Stress/strain respons is noted as solid lines, while electrical response appears as dotted lines. Insets are used to display electrical response effects that are not apparent at the main figure scale. It should be noted that the included graphs only show through 0.35 strain, as this region exists before electrodes began to fail. It can also be noted that the exposed samples show two distinct behaviors, with one failing much earlier than the other. This is consistent with observations across the complete sample set, where about half of the tested samples followed each failure mode.

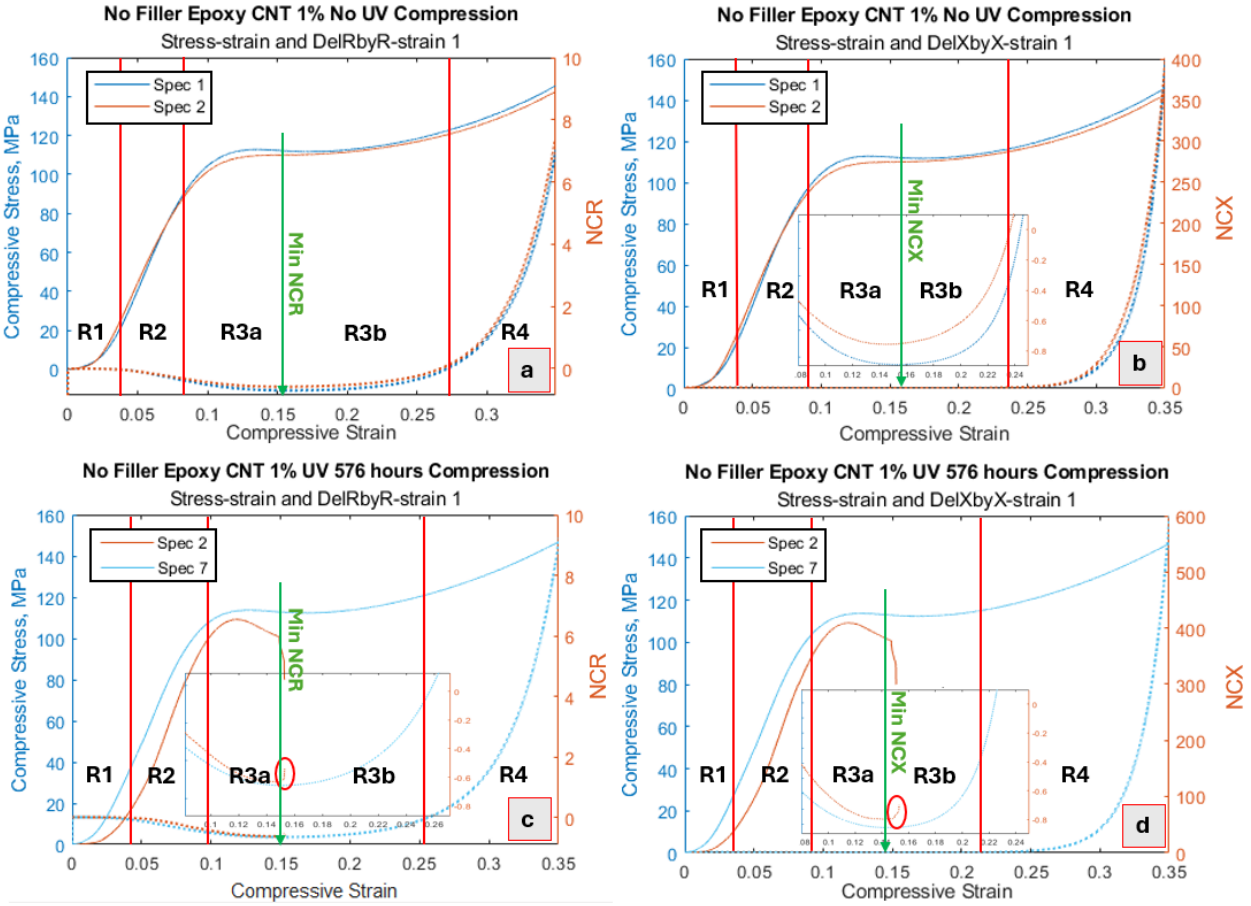

Figure 5: Mechanical and electrical response of unexposed (a-b) and 576 hour UV exposed (c-d) epoxy/1% CNT samples. Regions of interest and minimums noted.

NCR anc NCX data for both sample sets show strong strain and damage sensing response. Sample response can be divided into four major regions R1-R4. R1 is the region where instabilities caused by electrode inconsistencies and sample seating or geometric irregularities are allowed to stabilize. In R2, both mechanical and electrical data shows a primarily linear response in the material elastic regime as magnitudes of resistance and reactance decrease with compressive strain due to geometric effects. In R3a, the negative slope in electrical data indicative of this elastic response begins to flatten as microscale damage disrupts CNT networks and leads to an increase in the magnitude of resistance or reactance values. In R3b, which begins at the minimum NCR or NCX value, this damage influence begins to overcome the strain response. At the beginning of R4, the response is damage-dominated, as both resistance and reactance magnitudes increase past their initial baselines, and the slopes of both NCR and NCX (often referred to as the gauge factor) consistently increase with further network disruption and increases in relative resistance and reactance magnitudes regardless of strain.

Both NCR and NCX have similar linear responses, and both also detect macrodamage events as can be seen in the spikes in specimen 2 values in the insets in Fig. 5 c-d (circled in red). It should also be noted that NCX response is several orders of magnitude greater than NCR response in R4, which suggests a higher sensitivity to micro-damage accumulation.

One significant difference between exposed and unexposed samples was the disposition toward early failure events in exposed samples, likely brought on by embrittlement and fracture of surface layers resulting from UV degradation. Such behavior would create stress concentrations and provide impetus for crack propagation throughout the sample.

Conclusions and Future Work

This study confirms that strain and damage sensing capabilities persist after significant exposure of epoxy/CNT specimens to UV radiation. While changes in mechanical behavior exist in exposed samples, useful SHM information can still be obtained from analysis of NCR and NCX data. This shows that such composites may still be applied in environments with high UV exposures, such as the Lunar surface.

Future work will involve a more rigorous analysis of NCR and NCX behavior, including correlation of material properties, such as non-linear onset strain and modulus, with associated electrical response. Gauge factors will also be examined in greater detail and used to provide a more holistic characterization of sensing behavior. The noted epoxy/CNT composite will next be used as a binder in epoxy/CNT/Lunar regolith simulant samples to confirm if SHM capabilities persist with high loadings of regolith particulate. Composition will be varied as necessary to achieve useful electrical comparisons while maintaining binder contents $<20\%$ to allow for decreased launch mass of materials transported to the Lunar surface. These polymer-bonded regolith composites will also be subjected to low temperatures to confirm functionality in thermal conditions similar to those which may be experienced during future missions.

Acknowledgements

This research would not have been achieved without the involvement of many experts. The author would like to thank Dr. Gary D. Seidel for lab technique and equipment training, access to the Aerospace Structures and Materials Laboratory, material acquisition, and general research support and critiquing. Viswajit Talluru and Nishant Shirodkar assisted in best practice lab and instrumentation trainings, while Brett Segal as-

sisted in the fabrication and testing of sample sets.

The author would also like to acknowledge the financial support for this research obtained from the Virginia Space Grant Consortium Graduate STEM Research Fellowship, the Joseph Frank Hunkler Memorial Scholarship, and the Graduate Research Development Program (GRDP) Fund.

Works Cited

[1] C. W. Warner. Lunar Living: NASAs Artemis Base Camp Concept. URL: blogs.nasa.gov/artemis/2020/10/28/lunar-living-nasas-artemis-base-camp-concept/. (published: 10.28.2020).

[2] National Aeronautics and Space Administration. NASA Technology Roadmaps TA 10: Nanotechnology. URL: nspires . nasaprs . com / external / viewrepositorydocument / cmdocumentid=896240/solicitationId=%5C % 7B4C4796B7 - 1D86 - C986 - 49E5 - A76ABB0A9EAE % 5C % 7D / viewSolicitationDocument = 1 / 2015 _ NASA _ Technology _ Roadmaps _ TA10 _ Nanotechnology . pdf. (published: 07/2015).

[3] R. Katam, V. D. K. Pasupuleti, and P. Kalapatapu. "A review on structural health monitoring: past to present". In: Innovative Infrastructure Solutions 8 (248 2023). DOI: 10.1007/s41062-023-01217-3.

[4] P. M. Ferreira et al. "Embedded Sensors for Structural Health Monitoring: Methodologies and Applications Review". In: Sensors 22 (2022), p. 8320. DOI: 10.3390/s22218320.

[5] V. Talluru and G. D. Seidel. "Experimental investigation of strain and damage sensing of polymer bonded energetic with MWCNTs and conductive grains under cyclic compressive loads". In: AIAA SciTech Forum. National Harbor, MD. 2023.

[6] J. J. Ku-Herrera, F. Aviles, and G. D. Seidel. "Self-sensing of elastic strain, matrix yielding and plasticity in multiwall carbon nanotube/vinyl ester composites". In: Smart Materials and Structures 22 (2013).

[7] E. C. Sengezer and G. D. Seidel. "Structural Health Monitoring of Nanocomposite Bonded Energetic Materials Through Piezoresistive Response". In: AIAA Journal 56.3 (Mar. 2018).

[8] N. P. Shirodkar. "Leveraging Carbon based nanoparticle dispersions for fracture toughness enhancement and electro-mechanical sensing in multifunctional composites". PhD thesis. Virginia Polytechnic Institute and State University, 2022.

[9] J. Chen et al. "An overview of stretchable strain sensors from conductive polymer nanocomposites". In: Journal of Materials Chemistry C 7 (38 2019), pp. 11710–11730. DOI: 10 . 1039 / c9tc03655e.

[10] Xiao Su et al. "A comparative study of polymer nanocomposites containing multi-walled carbon nanotubes and graphene nanoplatelets". In: Nano Materials Science (2021). ISSN: 2589-9651. DOI: https : / / doi . org / 10 . 1016 / j . nanoms . 2021 . 08 . 003. URL: https : / / www . sciencedirect . com / science / article/pii/S2589965121000611.

[11] N. Shirodkar and G. D. Seidel. "Strain and damage sensing of polymer bonded mock energetics via piezoresistivity from carbon nanotube networks". In: AIAA SciTech Forum. Orlando, FL. 2020.

[12] S. Shirodkar N.and Rocker and G. D. Seidel. “Strain and damage sensing of polymer bonded mock energetics via piezoresistivity from carbon nanotube networks”. In: Smart Materials and Structures 28 (Sept. 2014).

[13] E. Yousif and R. Haddad. “Photodegradation and photostabilization of polymers, especially polystyrene: review”. In: SpringerPlus 2.398 (2013). URL: springerplus.com/content/2/1/398.

[14] X. Gu et al. “Probing photodegradation beneath the surface: a depth proling study of UV-degraded polymeric coatings with microchemical imaging and nanoindentation”. In: Journal of Coatings Technology and Research 4.4 (2007), pp. 389–399. DOI: 10 . 1007 / s11998-007-9052-x.

[15] M. M. Khotbehsara et al. “Effects of ultraviolet solar radiation on the properties of particulate-lled epoxy based polymer coating”. In: Polymer Degradation and Stability 181 (2020). DOI: 10 . 1016 / j . polymdegradstab . 2020 . 109352.

[16] F. Awaja and P. J. Pigram. “Surface molecular characterisation of different epoxy resin composites subjected to UV accelerated degradation using XPS and ToF-SIMS”. In: Polymer Degradation and Stability 94 (2009), pp. 651–658. DOI: 10.1016/j.polymdegradstab.2009.01.001.

[17] E. J. Petersen et al. “Methods to assess the impact of UV irradiation on the surface chemistry and structure of multiwall carbon nanotube epoxy nanocomposites”. In: Carbon 69 (2014), pp. 194–205.

[18] T. Nguyen et al. “Impact of UV irradiation on multiwall carbon nanotubes in nanocomposites: Formation of entangled surface layer and mechanisms of release resistance”. In: Carbon 116 (2017), pp. 191–200.

[19] Solar Constant and Zero Air Mass Solar Spectral Irradiance Tables. Standard. American Society for Testing and Materials, 2019.

[20] P. Gläser et al. “Illumination conditions at the lunar south pole using high resolution Digital Terrain Models from LOLA”. In: Icarus 243 (Nov. 2014), pp. 78–90. DOI: 10.1016/j.icarus.2014.08.013.

[21] J. Lucas. What Is Ultraviolet Light? (cited: 03/2024). URL: https://www.livescience . com / 50326 - what - is - ultraviolet - light . html. (published: 09/2017).

[22] Resolution Performance Products. Product Bulletin: EPIKOTE Resin 862/EPIKURE Curing Agent W System. Sept. 2022. URL: miller - stephenson . com / wp - content / uploads / 2016 / 08 / W . pdf (visited on 10/14/2022).

[23] MasterBond. Low Temperature Serviceability. (cited: 09/2021). URL: masterbond . com / properties / low - temperature-serviceability.

[24] MasterBond. Safety Data Sheet (EP29LPSP Part-A). obtained by request. 2019. URL: masterbond . com / tds/ep29lpsp (visited on 10/22/2022).

[25] MG Chemicals. 8331D - Silver Conductive Epoxy Adhesive. (cited: 08/2023). 2023. URL: https : / / mgchemicals . com / products / adhesives / electrically-conductive-adhesives/silver-epoxy/.

[26] World Health Organization. Radiation: Ultraviolet (UV) radiation. Mar. 2016. URL: http://who.int/news-room/questions-and-answers/item/radiation-ultraviolet-(uv) (visited on 10/22/2022).

[27] Cross-program Design Specification for Natural Environments (DSNE). Standard. NASA, Dec. 2019.

[28] NASA. Lunar Surface Solar Array Structures. Sept. 2020. URL: sbir.gov/node/1836151.

[29] R. L. Lucke, R. C. Henry, and W. G. Fastie. "Far-ultraviolet albedo of the Moon". In: The Astronomical Journal 81.12 (1976), pp. 1162–1169.

[30] J. Cunningham and G. D. Seidel. "Damage Sensing Enhancement in Polymer-Regolith-CNT Composites via Exposure to UV Radiation–Foundational Work". In: Virginia Space Grant Consortium (VSGC) Student Research Conference. Hampton, VA. 2023.

[31] C. Yoder. Common Bond Energies (D) and Bond Lengths (r). 2022. URL: http://wiredchemist.com/chemistry/data/bond_energies_lengths.html (visited on 10/22/2022).

[32] University of Michigan. PDMS. Apr. 2020. URL: http://lnf-wiki.eecs.umich.edu/wiki/PDMS (visited on 10/22/2022).

[33] A. Neogi, N. Mitra, and R. Talreja. "Cavitation in epoxies under composite-like stress states". In: Composites: Part A 106 (2018), pp. 52–58. DOI: 10.1016/j.compositesa.2017.12.003.

[34] PVEducation. Energy of Photon. URL: http://pveducation.org/pvcdrom/properties-of-sunlight/energy-of-photon (visited on 10/26/2022).